J. Condensed Matter Nucl. Sci. 3 (2010) 77–92

Research Article

Analysis of some experimental data from the two-laser experiment

Peter L. Hagelstein*
Research Laboratory of Electronics, Massachusetts Institute of Technology, Cambridge, MA 02139, USA

Dennis G. Letts
12015 Ladrido Lane, Austin, TX 78727, USA

Abstract

We consider simple relaxation models for fitting data from two-laser experiments. The approach has been used to analyze the data systematically from many data sets. A result of the fitting is that we find that the excess power responds quickly near 8 THz, and slowly near 15 and 21 THz.

Keywords: Data analysis, Excess heat, Fleischmann–Pons experiment, Optical phonons, Two-laser experiment

1. Introduction

In a recent set of experiments where two lasers were used to stimulate excess power in Pd cathodes, the response was observed to depend on the difference frequency between the two lasers which was at THz frequencies [1]. The response was found to be largest at three different "sweet spots", corresponding to 8.2, 15.1, and 20.8 THz. The first two frequencies appear to be connected to low group velocity compressional modes in PdD. The origin of the third frequency is less clear. Possible explanations include H contamination in PdD, and optical phonon modes associated with D in vacancies in Au [2].

In this work, we are concerned with the issue of data analysis. In previous work, we reported results for the excess power increase by first determining the excess power before the lasers turned on (or changed difference frequency), and then estimating the increase in the excess power after about 3 h [1]. A weakness of this approach is that the different estimates are subjective, and it is not so easy to determine the associated error bars. This issue was raised recently by a reviewer when we submitted a paper for publication.

*E-mail: plh@mit.edu

The application of statistical methods systematically to the experimental data is in principle straightforward. However, there are issues, some of which are interesting. One approach might be to develop statistical estimates for the excess power before the stimulation, then wait for a steady state to be attained, and then do a second statistical estimate for the excess power. In either case, we need to correct for the response of the system to the absorbed laser power.

However, there is much more information that is potentially present in the data. For example, how long does it take to reach a steady state, and what kind of function [2] describes the dynamics? Are the dynamics the same in the different experiments, or does the system respond faster in some cases than in others? Then, if we understood the dynamics, would it change our picture the system? Interesting questions, but whether we are able to answer them or not depends on the degree to which the data differentiates between different models.

In what follows, we consider two different models that we have used to fit the data. We also consider two different data sets where excess power was observed.

2. Calorimeter Response

The calorimetry used in the experiments is simple Fick's law calorimetry with no dynamical correction (these and other issues are discussed in [2]). The output power is computed from measurements of the temperature difference inside and outside of the cell

$$P_{\rm out} \;=\; K\,\Delta T. \tag{1}$$

The input power for the present discussion is a combination of the electrical input power minus the contribution due to splitting of heavy water into deuterium and oxygen

$$P_{\rm in} \;=\; I\,(V - V_0), \tag{2}$$

where V_0 is the thermoneutral potential.

The cell is run in a constant current mode from minute to minute, and an approximate constant power condition is obtained by updating the current each minute so that the product of the new current times the old voltage will be matched to the desired electrical input power. As a result, there are minor fluctuations in the input power.

Of course, the calorimeter will respond to changes in the input with a delay since there is a significant heat capacity. Since this is not taken into account by the simple Fick's law calorimetry, we would expect that the Fick's law output power will relax to the input, as in the example of Fig. 1. We could take this into account by using an improved model for the calorimeter that is more complete, and make use of the sophisticated method presented by Miles and Fleischmann [3]. However, the goal of this present work is to bring out some interesting features of the experimental results, rather than to develop a better model for the calorimeter.

2.1. Fitting the output power

In the most simplistic point of view, the model output power should have the form

$$P_{\rm out} \;=\; P_{\rm in}\,\left(1 - {\rm e}^{-t/\tau}\right), \tag{3}$$

where τ is the associated relaxation time. This suggests that we should use a fitting function of the form

$$P_{\rm out} \;=\; A + B\,{\rm e}^{-t/\tau}. \tag{4}$$

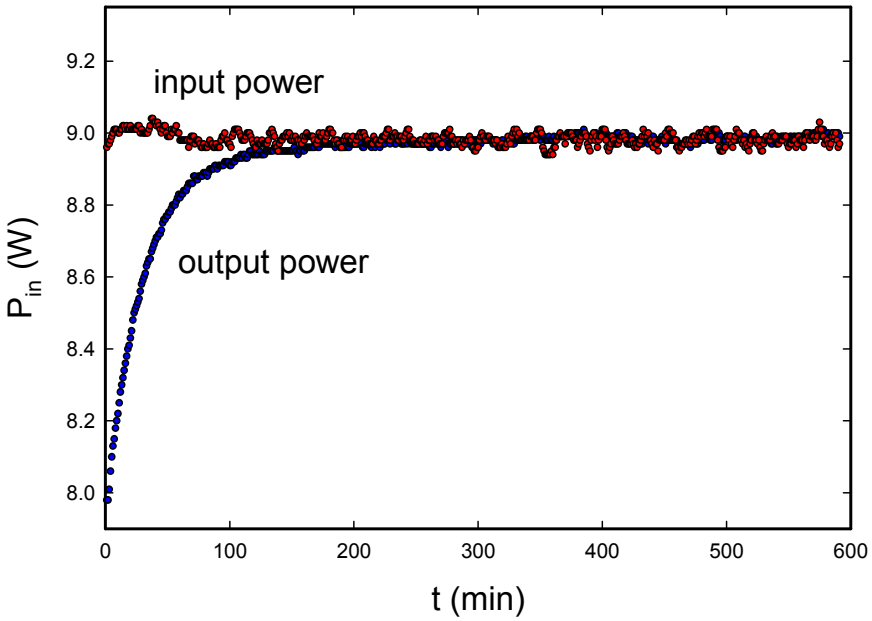

Figure 1. Input and output power points from DGL662v2.

The results from the fitting are

$$A = 8.98\ \text{W}, \qquad B = -1.06\ \text{W}, \qquad \tau = 31.9\ \text{min}. \tag{5}$$

The experimental points and the associated fit are shown in Fig. 2. We computed the variance according to

$$\text{var} = \frac{1}{N}\sum_i [P_i - P_{\text{fit}}(t_i)]^2. \tag{6}$$

The square root of the variance for this fit is

$$\Delta P = \sqrt{\text{var}} = 11.3\ \text{mW}. \tag{7}$$

2.2. Drift

There is a drift evident in the calibration data. We can fit the drift according to

$$P_{\text{out}} = A + B\, \text{e}^{-t/\tau} + Ct. \tag{8}$$

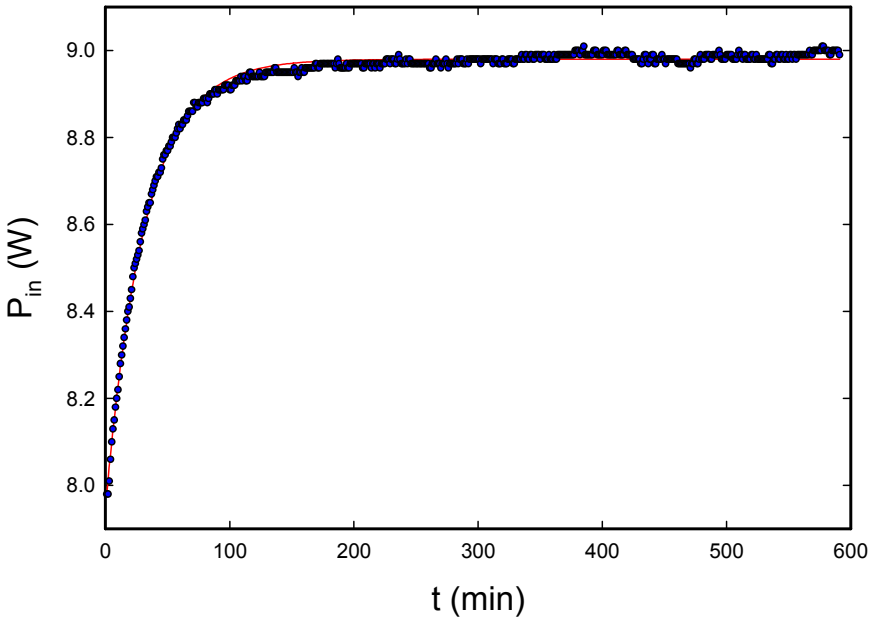

Figure 2. Output power points and fit for DGL662v2.

The fitting parameters that result are

$$A = 8.95\ \text{W}, \qquad B = -1.02\ \text{W}, \qquad C = 7.9 \times 10^{-5}\ \text{W/min}, \qquad \tau = 29.2\ \text{min}. \tag{9}$$

The associated spread in the excess power is

$$\Delta P = \sqrt{\text{var}} = 8.17\ \text{mW}. \tag{10}$$

A relevant question here is why there should be a drift in the data. One possibility is that perhaps a drift is present in the input power. To test this we show the input power in Fig. 3. Inspection of this figure indicates that there is no significant drift at late times, so that the origin of the drift lies elsewhere.

3. Absorbed Laser Power

In the calorimetric approach used, most of the excess power that is seen appears to be due to anomalous power production by the cathode. We need to correct for the absorbed laser power, since it results in a temperature increase on a similar footing to the excess power production. The amount of laser power absorbed is small in comparison to the excess power production generally near resonance. In earlier work, we neglected the absorbed laser power. In response to comments from a reviewer we expand our discussion here to include the effect.

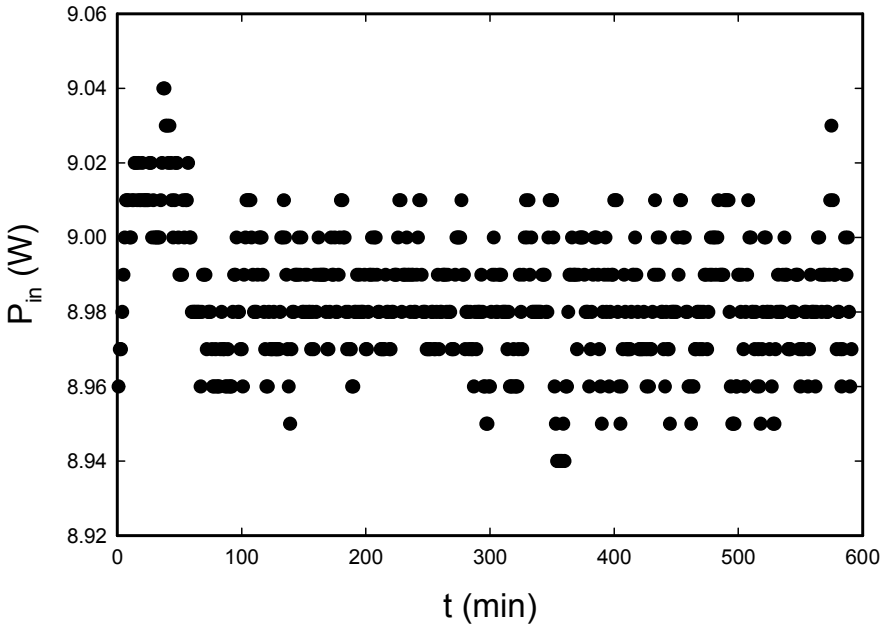

Figure 3. Input power points from DGL662v2.

In the set of experiments for which we have excess power data, the amount of laser light absorbed was not measured separately in each case. From a theoretical viewpoint, we expect the absorption of the cathode to be dominant. Hence, all that we need to do is to first estimate what fraction of the laser light makes it to the cathode, and then determine the fraction absorbed. When new (before 2002), each laser could produce up to 30 mW, but recent measurements indicate that the laser power has degraded so that the total incident power from both is about 25 mW. The incident light passes through a double-pane glass window, then air, then the borosilicate glass of the cell, and finally the electrolyte prior to reaching the cell. We would expect roughly 90% of the incident light to reach the cathode surface.

The fraction of the incident light absorbed is then dominated by the absorption at the cathode, which we discuss next. To get some intuition, we can use the Fresnel reflection coefficient appropriate for light incident on a metal in water, which we develop in the Appendix. If the cathode surface were pure Pd, then we could take the optical data from clean Pd in vacuum to arrive at an absorption coefficient of about 43% at 45^o (or about 39% of the laser radiation) for TM polarized light. In experiments in vacuum, the reflection is seen to be changed significantly due to the presence of an oxide layer. We would expect the cathode surface in the electrolyte to have a surface coating due to the electrolyte and electrochemistry, so that we would not be surprised if the measured number were different.

In the two-laser experiments we can look at the calorimetric results from experiments in which the lasers were turned on off of resonance, where the cell response is the smallest. An example of this is experiment 662I2, where data near the time when the lasers first turned on is shown in Fig. 4. The beat frequency in this case is 18.23 THz, which is in the dead region of the spectrum between the resonances at 15 and 21 THz. We see in this case a noisy calorimetric response with a relaxation time close to that of the calorimeter. This result is consistent with an absorption of 15 mW

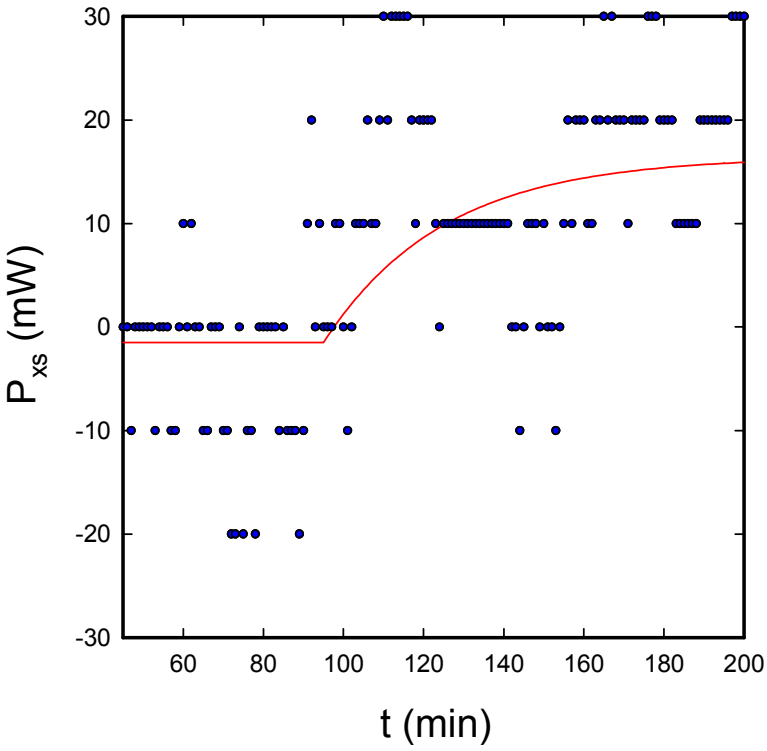

Figure 4. Data from experiment 662I2 around the laser turn on time.

of laser power. This is the number that we have adopted for the analysis of [2].

Subsequently, a calorimetric experiment in light water was run using one of the cathodes from the campaign in order to verify the absorbed power. In this experiment, one laser set at 659 nm was measured at 14.8 mW, the other set at 689 nm was measured at 11.5 mW, and the calorimeter (with no electrochemical input power) registered 15 mW of absorbed power (57% of the laser power was absorbed). In this case the lasers were both polarized in p-polarization. Changing to s-polarization was found not to impact the absorbed power. In the remainder of this paper we will neglect the absorbed laser power, since it provides a relatively small correction for the examples considered below.

4. Excess Power Event

We have focused on data from DGL662n and DGL662o combined since it provides one of the cleanest examples of excess power in the two-laser experiments. In this experiment, the cell was run for an extended period prior to turning on the two lasers, and a reasonably large excess power event was stimulated.

In the two-laser experiments, there sometimes appears an artifact shortly after the lasers turn on as a precursor to an excess power event. We know that it is an artifact since it is much shorter than the response time of the calorimeter.

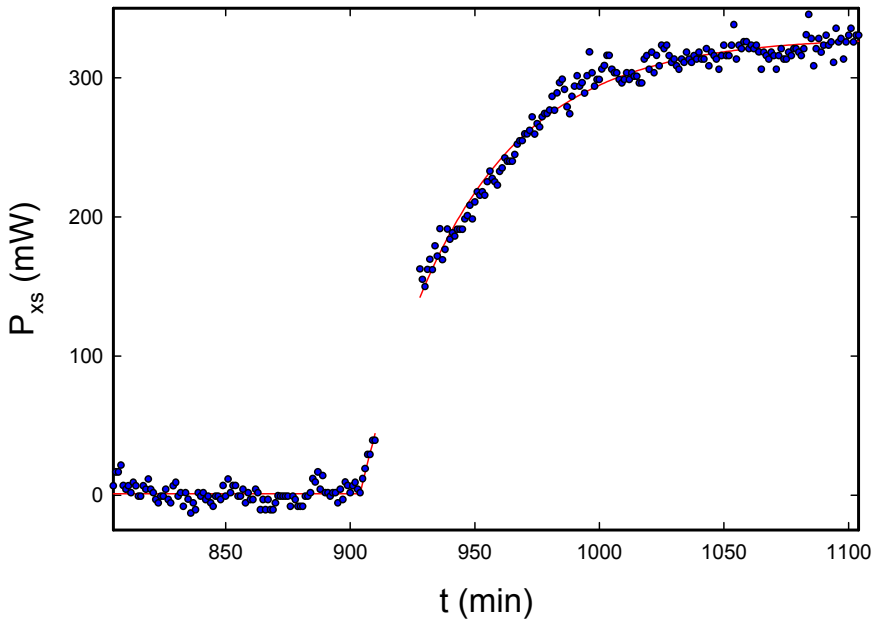

Figure 5. Excess power and fit for DGL662n and DGL662o, with the points removed around the artifact.

Measurements of the cell parameters indicates that this artifact is due to a sudden and sustained drop in the cell voltage, which leads to a temporary drop in the cell input power that is largely corrected within 10–15 min. Why the cell voltage drops is at present unknown.

4.1. Simple relaxation model

The simplest possible model that we might use is one that assumes relaxation for a step input. The excess power in such a model might look like

$$P_{\rm xs} \;=\; P_0 \left(1 - {\rm e}^{-(t-T_0)/\tau}\right) u(t - T_0), \tag{11}$$

where T_0 is the initiation time, P_0 the constant excess power source in the model, and $u(t)$ is the unit step function. This suggests that we try a fit of the form

$$P_{\rm fit} \;=\; A + B \,\left(1 - {\rm e}^{-(t-T_0)/\tau}\right) u(t - T_0). \tag{12}$$

We have removed some data around the artifact in order to obtain a fit that is less biased. The resulting fit is shown in Fig. 5, and the associated fitting parameters are

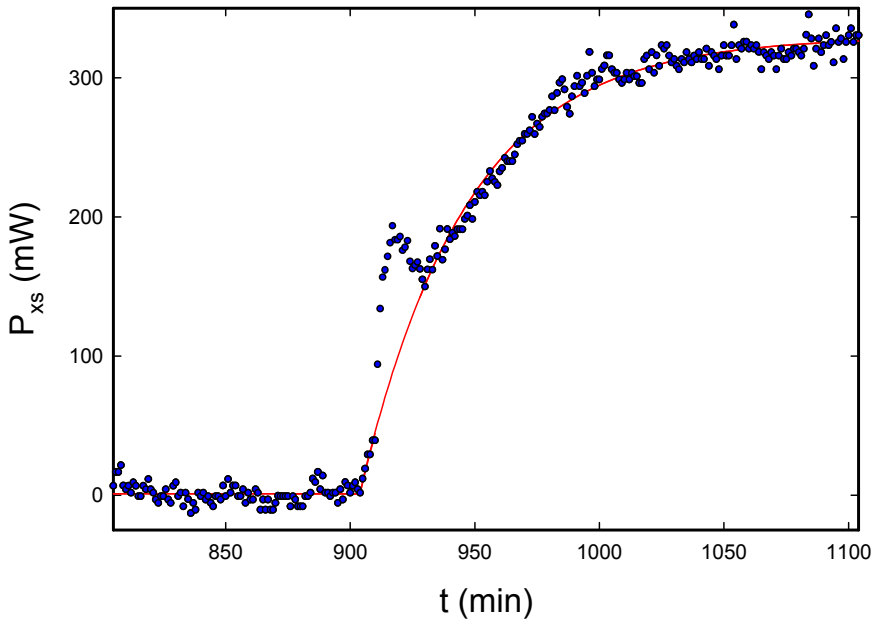

Figure 6. Excess power and fit for DGL662n and DGL662o including drift, shown with all experimental points in the time segment used.

$$A = 1.20\,\text{mW}, \qquad B = 328.24\,\text{mW}, \qquad T_0 = 904.0\,\text{min}, \qquad \tau = 42.71\,\text{min}. \tag{13}$$

Note that the relaxation time here is significantly longer than the calorimeter relaxation time. The spread in excess power as computed above is

$$\Delta P = 7.54\,\text{mW}. \tag{14}$$

4.2. Drift

We know that the calorimeter drifts from our experience with the calibration data. It is reasonable to redo the calculation assuming that there is a linear drift for this data set. To include a linear drift, we fit according to

$$P_{\text{fit}} = A + B\left(1 - \text{e}^{-(t-T_0)/\tau}\right)u(t-T_0) + C(t-T_0). \tag{15}$$

The resulting fitting parameters are

$$A = 3.58\,\text{mW}, \qquad B = 326.58\,\text{mW}, \qquad C = -2.91 \times 10^{-3}\,\text{mW/min},$$

$$T_0 \;=\; 904.1 \text{ min}, \qquad \tau \;=\; 43.04 \text{ min}. \tag{16}$$

This fit is shown compared with the data sets (including artifact) in Fig. 6. The associated spread in excess power is

$$\Delta P \;=\; 7.53 \text{ mW}. \tag{17}$$

We find that including the spread in this case changes the results at the per cent level.

4.3. Fewer points

In the computations above, we took points to 100 min before, and 200 min after. If we shorten these numbers to 70 min before and 150 min after, then we obtain

$$A \;=\; 4.12 \text{ mW}, \qquad B \;=\; 329.80 \text{ mW}, \qquad C \;=\; -4.83 \times 10^{-3} \text{ mW/min},$$
$$T_0 \;=\; 903.9 \text{ min}, \qquad \tau \;=\; 44.43 \text{ min} \tag{18}$$

with a smaller associated spread

$$\Delta P \;=\; 7.36 \text{ mW}. \tag{19}$$

5. Three-parameter Model

At this point, we have had an opportunity to apply the model and ideas above to many data sets, with the result that largely things work reasonably well. However, there remains an issue that we are motivated to address. We know that there is a characteristic response of the calorimeter to excess power sourced within the calorimeter. Yet in the model fit that we used above, we find that the relaxation time is often longer than the relaxation time of the calorimeter. If we de-convolve the associated signal, we end up with a source history that is highly constrained. It is possible to develop a more sophisticated three-parameter fit which relaxes the associated constraint.

5.1. Relaxation model

This motivates us to revise our model so as to include the basic calorimeter response, and then parameterize whatever is left over in terms of the underlying excess power signal. We consider the simplest relaxation model described by

$$\frac{\mathrm{d}}{\mathrm{d}t}P + \frac{P}{\tau_0} \;=\; \frac{P_\mathrm{s}}{\tau_0}. \tag{20}$$

Here P_s is the source excess power, and P is the excess power signal reported by the model calorimeter. We can express the calorimeter version of the power P in terms of the source version of the power P_s according to

$$P(t) \;=\; \int_{-\infty}^{\infty} P_\mathrm{s}(t')h(t-t')\mathrm{d}t', \tag{21}$$

where $h(t)$ is the impulse response

$$h(t) \;=\; \frac{\mathrm{e}^{-t/\tau_0}}{\tau_0}u(t). \tag{22}$$

5.2. Simple model based on a step

Now we are free to develop a model calorimeter power response based on a source power model. For example, if we chose a step

$$P_{\rm s}(t) \;=\; P_0 u(t). \tag{23}$$

Then we would obtain a calorimeter power given by

$$\begin{aligned} P(t) \;&=\; \int_{-\infty}^{\infty} P_0 u(t') \, \frac{{\rm e}^{-(t-t')/\tau_0}}{\tau_0} u(t-t') \, {\rm d}t' \\ &=\; u(t) P_0 {\rm e}^{-t/\tau_0} \int_0^t \frac{{\rm e}^{t'/\tau_0}}{\tau_0} {\rm d}t' \;=\; u(t) P_0 (1 - {\rm e}^{-t/\tau_0}). \end{aligned} \tag{24}$$

This is closely related to the fitting function that we selected, but in this version the τ_0 parameter is fixed by the calorimeter response rather than being determined by the data.

5.3. Source power for the model above

The natural question occurs as to what is the source assumed with the model that we discussed above. For this model, if we neglect the constant or linear offset, we might write

$$P(t) \;=\; B u(t) \left(1 - {\rm e}^{-t/\tau}\right). \tag{25}$$

The associated source power that would correspond to this is

$$P_{\rm s}(t) \;=\; P(t) + \tau_0 \frac{{\rm d}P}{{\rm d}t} \;=\; u(t) B \left[1 - \left(1 - \frac{\tau_0}{\tau}\right) {\rm e}^{-t/\tau}\right]. \tag{26}$$

We can recast this as

$$P_{\rm s}(t) \;=\; u(t) B \left(1 - \frac{\tau_0}{\tau}\right) \left(1 - {\rm e}^{-t/\tau}\right) + u(t) B \frac{\tau_0}{\tau}. \tag{27}$$

There is an initial step along with a relaxation curve. The amplitude of the step in this model is fixed by the ratio of the relaxation times.

5.4. More general model

Based on the argument above, it seems that we should be able to put together a better model based on separate parameters for the step and relaxation terms. For example, we might adopt a source power model of the form

$$P_s(t) \;=\; u(t) B \left(1 - {\rm e}^{-t/\tau}\right) + u(t) D. \tag{28}$$

The corresponding calorimeter power is

$$P(t) = \int_{\infty}^{\infty} P_s(t')h(t-t')\mathrm{d}t'$$

$$= u(t)(B+D)\left(1-\mathrm{e}^{-t/\tau_0}\right) - u(t)B\frac{(\mathrm{e}^{-t/\tau}-\mathrm{e}^{-t/\tau_0})}{\left(1-\frac{\tau_0}{\tau}\right)}. \quad (29)$$

6. Fitting Data with the Three-parameter Model

In order to tell whether the revised model helps, we need to try it on some data sets. The reference data set is a good data set generally, but in order to develop a useful fit, we need to remove some of the points around the artifact. As such, we would not expect to see much difference between the different models since the points where the models would show the difference is in the excluded region. Better is to test a different data set that is free of the artifact.

6.1. Reference data set

We begin by considering the reference data set. We have fit the data (with no drift), and we have obtained the following fit parameters

$$A = 1.57\,\mathrm{mW}, \qquad B = 110.67\,\mathrm{mW}, \qquad D = 214.33\,\mathrm{mW},$$

$$\tau_0 = 30.0\,\mathrm{min}, \qquad \tau = 33.45\,\mathrm{min} \quad (30)$$

with T_0 fixed at 904. The associated spread in excess power is

$$\Delta P = 7.52\,\mathrm{mW}. \quad (31)$$

This model gives results that are pretty similar to what we found previously.

6.2. Example without an artifact

In the different data sets, there occur examples that are fit well by a step function source model, and also examples that are fit by a dynamic source function. One example of a data set with a dynamic source function is DGL670a, which was listed as point 42 on the earlier table at 19.28 THz, but which was subsequently corrected to 13.45 THz. The fitting parameters in this case are

$$A = 6.49\,\mathrm{mW}, \qquad B = 66.15\,\mathrm{mW}, \qquad D = 18.52\,\mathrm{mW},$$

$$\tau_0 = 30.0\,\mathrm{min}, \qquad \tau = 54.69\,\mathrm{min} \quad (32)$$

with T_0 taken to be 8266. The associated spread in excess power is

$$\Delta P = 6.16\,\mathrm{mW}. \quad (33)$$

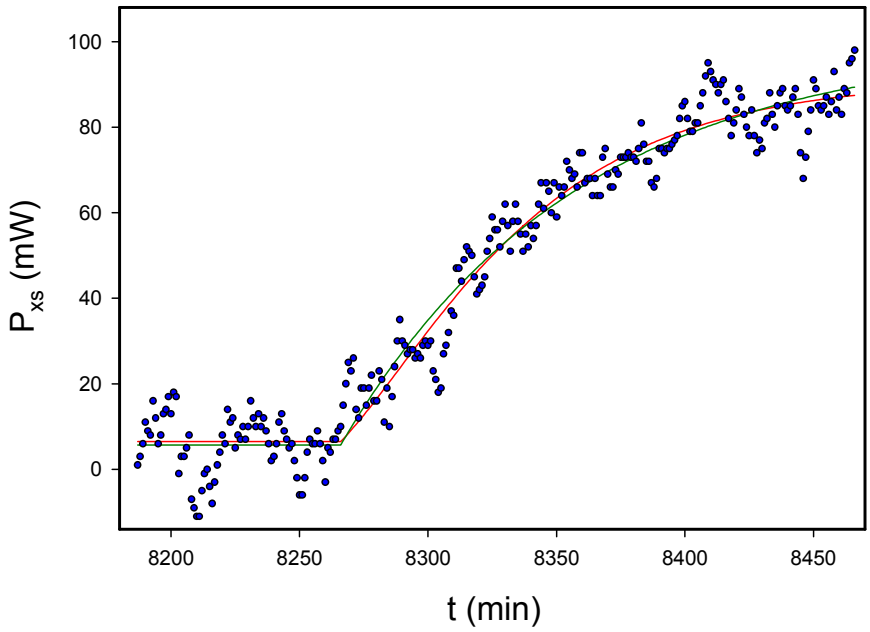

Figure 7. Excess power and fit for DGL670a using the three-parameter model (*red*) compared with the optimized simple model (*green*).

However, having made arguments in favor of a slowed onset, in fairness we need to also argue the other side as well. In this case, the simpler model also gives reasonable results, as shown in Fig. 7. In this case the fitting parameters are

$$A = 5.78\ \text{mW}, \qquad B = 0\ \text{mW}, \qquad D = 94.84\ \text{mW},$$

$$\tau = 92.97\ \text{min} \tag{34}$$

with

$$\Delta P = 6.30\ \text{mW}. \tag{35}$$

This model gives a higher estimate for the source power, and a poorer fit to the data.

Results for both models are shown in Fig. 7. It is possible to see the effect of the slower rise in the associated curve for the three-parameter model relative to the simpler model. Unfortunately, since the two different models lead to curves that are close together, it is unlikely that one could make a compelling case that the data requires the more sophisticated model. If one uses the more sophisticated model, it seems unlikely that we would be sure that the parameters that provide an optimum fit tell us much about the source history, since we can obtain very similar curves with other parameters.

7. Discussion and Conclusions

There are a number of conclusions which might be drawn from the discussion of the previous sections. Perhaps the most notable conclusion is that in the two-laser experiments, the excess power appears to relax to a constant value (which depends on the difference frequency between the two lasers). This is different qualitatively from some of the early Fleischmann–Pons experiments in which the excess power often would occur in bursts with sometimes complicated histories. For the data sets considered here, a simple relaxation model can provide a good fit for the experimental data. We found this to be the case for the majority of the 18 data sets of this type that we analyzed.

A second important conclusion is that the relaxation time associated with the excess power response is usually longer than the calorimeter response time. We can conclude that the source excess power itself relaxes to a reasonably constant level over times ranging between a few minutes and 4 h. There does not seem to be a clear correlation between the relaxation time and the excess power level. There does seem to be a correlation between the relaxation time and the difference frequency (see Fig. 8). The three data sets near 8 THz show short relaxation times, where the source τ of the three-parameter model is less than 13 min. All but one of the other data sets associated with the 15 and 20 THz resonances have longer relaxation times, most above 30 min.

What this source relaxation time is due to is not known. There are two plausible scenarios that suggest themselves as possibilities. In one scenario, the two lasers are focused to a small spot on the cathode, and the lag time is associated with the spreading of the source from initially being localized to extending over a large fraction of the cathode surface

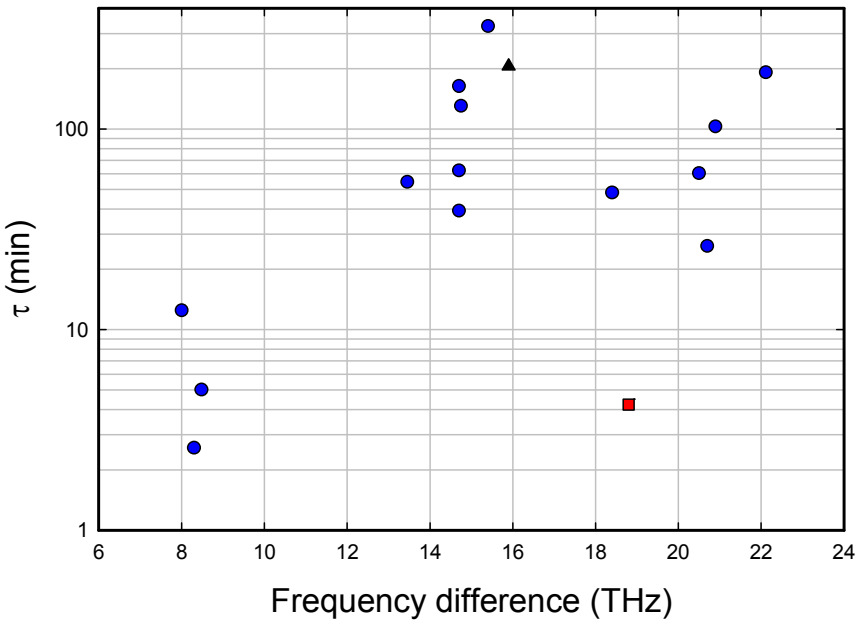

Figure 8. Source relaxation time parameter τ from three-parameter model fits of two-laser experiments. The data in blue circles are for the "normal" runs; the excess power was interrupted for the red square at 18.8 THz, so that the τ of 4.2 min is inaccurate; the data set is incomplete for the black triangle at 15.9 THz, so that the estimate of 206 min has a large uncertainty.

at late time. In another scenario, the response is delocalized in space from early time, but it is the amplitude that builds up. Simple calorimetric experiments cannot resolve between these scenarios. If the cathodes showed a response in the IR, as was the case in the Swartz experiments [4], then perhaps we would be able to see the surface area response change in time, and perhaps correlate with the excess power production.

If a faster calorimeter were used, then it would be possible to measure the excess power history and dynamics with more resolution. This would seem to be a good thing. If the short time response for the 8 THz frequency points is a real effect, and if the longer response for the 15 and 21 THz points is also real, then this might be useful to confirm and to study. Perhaps the system is telling us something helpful in this data.

Appendix A. Idealized Absorption Model

We are interested in developing a simple theoretical model for laser light absorption from a a model metal surface in the electrolyte. Our motivation for this is that such a model can shed light on how much absorption might be expected under conditions that are better understood than those of the experiment.

The light initially comes through air, then hits the outer glass cell, passes into the electrolyte, and then is absorbed and reflected at the cathode surface. We can analyze a simplified version of the problem using four homogeneous regions. Good optical data is available for palladium and for gold in vacuum, but the observed reflection or absorption depends also on surface contaminants and morphology. We estimate a relatively high absorption fraction from the optical data for a clean Pd surface.

Appendix A.1. TM absorption at a metal surface

In what follows we are interested in obtaining the relevant Fresnel equations to determine the absorption of a beam in heavy water on a metal surface, and separately the reflection associated with going from air through glass into heavy water. For TM light (which corresponds to p-polarization), we focus on the magnetic field. In the electrolyte we write

$$\mathbf{H} \;=\; \hat{y}\left[H_{\rm i}{\rm e}^{i(k_x x+k_z z)} + H_{\rm r}{\rm e}^{i(k_x x-k_z z)}\right]. \tag{A.1}$$

In the metal the electromagnetic field does not propagate because the laser frequency is below the plasma frequency. In this case we may write

$$\mathbf{H} \;=\; \hat{y}H_{\rm t}{\rm e}^{ik_x x}{\rm e}^{-\alpha z}. \tag{A.2}$$

In the absence of a surface current the (transverse) magnetic field is continuous across the boundary, so that

$$H_{\rm i} + H_{\rm r} \;=\; H_{\rm t}. \tag{A.3}$$

The transverse component of the electric field must also be continuous across the boundary, which leads to

$$\frac{k_z}{\omega\epsilon[{\rm D_2O}]}(H_{\rm i} - H_{\rm r}) \;=\; i\frac{\alpha}{\omega\epsilon[{\rm Pd}]}H_{\rm t}. \tag{A.4}$$

We can solve these simultaneously to obtain

$$r_{\rm TM}(\theta) \;=\; \frac{H_{\rm r}}{H_{\rm i}} \;=\; -\frac{\alpha\epsilon[{\rm D_2O}] + ik_z\epsilon[{\rm Pd}]}{\alpha\epsilon[{\rm D_2O}] - ik_z\epsilon[{\rm Pd}]}, \tag{A.5}$$

where $r_{\rm TM}$ is the reflection coefficient.

We can make use of the relations

$$\epsilon[{\rm D_2O}]\mu_0\omega^2 \;=\; k^2, \tag{A.6}$$

$$k_z \;=\; k\cos\theta, \qquad k_x \;=\; k\sin\theta, \tag{A.7}$$

$$-\epsilon[{\rm Pd}]\mu_0\omega^2 \;=\; \alpha^2 - k_x^2 \tag{A.8}$$

in order to rewrite $r_{\rm TM}$ as

$$r_{\rm TM}(\theta) \;=\; \frac{H_{\rm r}}{H_{\rm i}} \;=\; -\,\frac{\sqrt{\epsilon[{\rm D_2O}]\sin^2\theta - \epsilon[{\rm Pd}]}\epsilon[{\rm D_2O}] + i\sqrt{\epsilon[{\rm D_2O}]}\epsilon[{\rm Pd}]\cos\theta}{\sqrt{\epsilon[{\rm D_2O}]\sin^2\theta - \epsilon[{\rm Pd}]}\epsilon[{\rm D_2O}] - i\sqrt{\epsilon[{\rm D_2O}]}\epsilon[{\rm Pd}]\cos\theta}. \tag{A.9}$$

Since there is very little loss in the electrolye, the associated dielectric constant $\epsilon[{\rm D_2O}]$ is real to within an excellent approximation and positive. Since the laser light is below the plasma frequency of the cathode, the real part of the dielectric constant $\epsilon[{\rm Pd}]$ is negative. Since the metal is lossy, there will be a nonzero imaginary part of this dielectric constant.

A similar analysis for TE polarization leads to

$$r_{\rm TE}(\theta) \;=\; \frac{E_{\rm r}}{E_{\rm i}} \;=\; -\,\frac{\sqrt{\epsilon[{\rm D_2O}]\sin^2\theta - \epsilon[{\rm Pd}]} + i\sqrt{\epsilon[{\rm D_2O}]}\cos\theta}{\sqrt{\epsilon[{\rm D_2O}]\sin^2\theta - \epsilon[{\rm Pd}]} - i\sqrt{\epsilon[{\rm D_2O}]}\cos\theta}. \tag{A.10}$$

The fraction of the light absorbed in this part of the model is

$$f_{\rm abs}(\theta) \;=\; 1 - |r(\theta)|^2, \tag{A.11}$$

where r is taken to be one of the two expressions above depending on the polarization.

Appendix A.2. Optical constants and absorption

To proceed we require estimates for the dielectric constant of heavy water and for the cathode. We will adopt 665 nm as a reference laser wavelength for our estimates. The optical constant for light water is n is 1.331 [5] (we do not have data at present for heavy water in this spectral range), so that we will use for $\epsilon[{\rm D_2O}]$

$$\epsilon[{\rm D_2O}] \;=\; 1.77\,\epsilon_0, \tag{A.12}$$

The optical constants for Pd at 665 nm are $n = 1.81$ and $k = 4.38$ [6], so that for this calculation we can use

$$\epsilon[{\rm Pd}] \;=\; -\,15.9(1+i)\,\epsilon_0. \tag{A.13}$$

These optical data can be used to construct the absorption curve shown in Fig. 9. The absorption fraction at an incident angle of $45^{\rm o}$ is calculated to be 0.43.

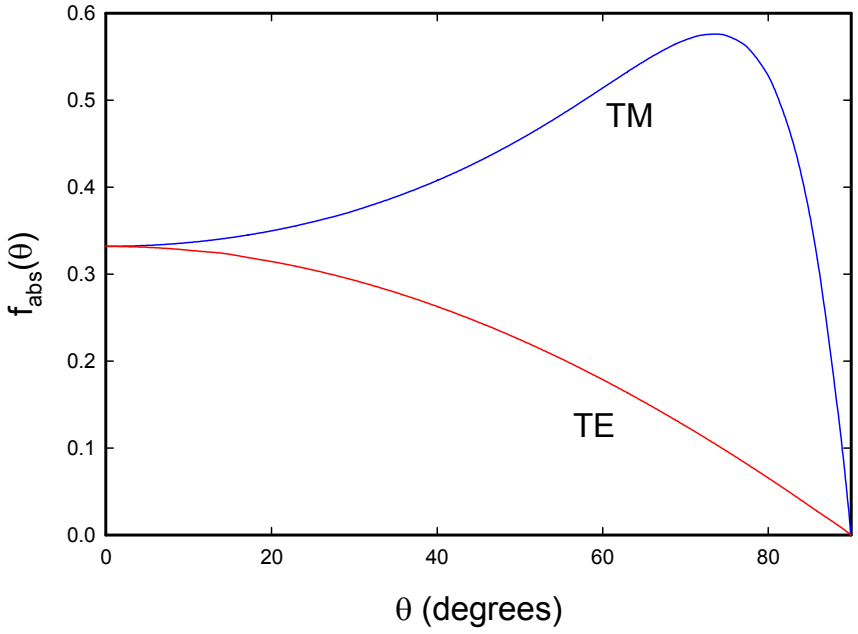

Figure 9. Absorbed TM and TE fraction of 685 nm light in water on Pd as a function of angle θ relative to normal.

We note that the absorption fraction shown in Fig. 9 is high, and that very clean surfaces in vacuum were used for the measurements of the optical constants that we used. It was noted in [6] that if the surface is oxidized, then a different amount of light is reflected (an oxide layer in vacuum decreases the reflection).

There is gold electroplated on the surface in the two-laser experiment. From the optical constants of metallic gold near 685 nm ($n = 0.14$ and $k = 3.76$ [7]), we would find an absorption fraction of about 0.025 for a planar gold surface.

References

[1] D. Letts, D. Cravens, and P.L. Hagelstein, Dual laser stimulation and optical phonons in palladium deuteride, in low-energy nuclear reactions and new energy technologies, *Low-Energy Nuclear Reactions Sourcebook*, Vol. 2, American Chemical Society: Washington DC, 2009, pp. 81–93.
[2] P.L. Hagelstein, D.G. Letts and D. Cravens, *J. Cond. Mat. Nucl. Sci.* **3** (2010) 59.
[3] M.H. Miles and M. Fleischmann, Accuracy of isoperibolic calorimetry used in a cold fusion control experiment, *Low-Energy Nuclear Reactions Sourcebook*, edited by J. Marwan and S. Krivit, 2009, p. 153.
[4] M.R. Swartz, G. Verner, A. Weinberg, Non-thermal near-IR emission linked with excess power gain in high impedance and codeposition phusor-LANR devices, *Proc. 14th International Conference on Condensed Matter Nuclear Science*, Washington, DC (in press).
[5] G.M. Hale and M.R. Querry, *Appl. Optics* **12** (1973) 553.
[6] P.B. Johnson and R.W. Christy, *Phys. Rev.* B **9** (1974) 5056.
[7] P.B. Johnson and R.W. Christy, *Phys. Rev.* B **6** (1972) 4370.